A Gas-Phase Kinetic Study of the Reaction between Bromine Monoxide and Methylperoxy Radicals at Atmospheric Temperatures

Shinichi Enami, Takashi Yamanaka, Tomoki Nakayama, Satoshi Hashimoto, and Masahiro Kawasaki*

Department of Molecular Engineering, Kyoto University, Kyoto 615-8510, Japan

Dudley E. Shallcross

Bristol Biogeochemistry Research Centre, School of Chemistry, Bristol, BS8 1TS, United Kingdom

Yukio Nakano and Takashi Ishiwata

Faculty of Information Sciences, Hiroshima City University, Hiroshima 731-3194, Japan

Received: December 6, 2006; In Final Form: February 1, 2007

The rate constant of the reaction of BrO with CH_3O_2 was determined to be $k_1 = (6.2 \pm 2.5) \times 10^{-12}$ cm^3 molecule^{-1} s^{-1} at 298 K and 100−200 Torr of O_2 diluent. Quoted uncertainty was two standard deviations. No significant pressure dependence of the rate constants was observed at 100−200 Torr total pressure of N_2 or O_2 diluents. Temperature dependence of the rate constants was further investigated over the range 233−333 K, and an Arrhenius type expression was obtained for $k_1 = 4.6 \times 10^{-13} \exp[(798 \pm 76)/T]$ cm^3 molecule^{-1} s^{-1}. The product branching ratios were evaluated and the atmospheric implications were discussed.

1. Introduction

The role of halogen cycles in shaping the composition of marine boundary layer (MBL) air has been the subject of intense study in recent years.[1−5] Halogen monoxide radicals, XO (X═Cl, Br, and I), are the key species of ozone-depleting cycles in the MBL and for Cl and Br are also known to be important in lower stratospheric ozone depletion. XO radicals react with HO_2, NO_2, and themselves and finally result in the regeneration of X atoms, which destroy ozone effectively. BrO has been widely observed at surface sites around the world, where appreciable levels have been reported. A maximum level of BrO of 6.5 pptv at Mace Head on the west coast of Ireland,[6] 17 pptv in the Arctic,[7] 30 pptv in the Antarctic,[8] and 200 pptv at the Dead Sea[9] show that the radical is widespread but also highly variable in level. Peroxy radicals, RO_2, are candidates for consumers of BrO since RO_2 have been measured in the MBL at mixing ratios of 10−40 pptv[10] and 40−80 pptv.[11] Recent experimental studies suggested that the reaction of IO with RO_2 could be involved in the important ozone depleting cycles in MBL.[12,13] However, the precise role of XO radicals in the MBL is still uncertain, because of the paucity of the knowledge of the reaction rate constants, especially for radical−radical reactions.

There has been only one experimental report on the kinetics of the reaction of BrO with CH_3O_2. The rate constant was reported to be $(5.7 \pm 0.6) \times 10^{-12}$ cm^3 molecule^{-1} s^{-1} at 298 K and 1 Torr total pressure of He diluent using a discharge-flow tube method by Aranda et al:[14]

$$CH_3O_2 + BrO \rightarrow CH_3O + Br + O_2 \quad (1a)$$

$$\rightarrow CH_3O + OBrO \quad (1b)$$

$$\rightarrow CH_2O_2 + HOBr \quad (1c)$$

$$\rightarrow CH_3OBr + O_2 \quad (1d)$$

They reported that the dominant reaction path is reaction 1c with the branching ratio of (0.8 ± 0.2) and the minor channels are 1a and 1b with the sum of the branching ratios being (0.3 ± 0.1). However, a recent theoretical study indicates that the most feasible pathway of the reaction of BrO with CH_3O_2 is the formation of CH_3OOOBr as an intermediate and its decomposition into CH_2O and HOOBr:[15]

$$CH_3O_2 + BrO \rightarrow CH_3OOOBr^* \rightarrow CH_2O + HOOBr \quad (1e)$$

Reactions 1a−1d are possible processes considering the analogous reactions of ClO with CH_3O_2,[16] and reaction 1e is the path predicted by theoretical calculation.[15]

In this paper we have measured the rate constants for the reaction of BrO with CH_3O_2 at 233 − 333 K and 100−200 Torr total pressure of N_2 or O_2 diluents using cavity ring-down spectroscopy (CRDS). The upper limit for the rate coefficient of the BrO formation path in the reaction of Br atoms with CH_3O_2 and the rate constant of the self-reaction of BrO were also determined. CRDS has been widely used in spectroscopic and kinetic studies for radical reactions, which are applicable to atmospheric modeling,[17−19] because CRDS is suitable for the experiments at wide ranges of pressure and temperature.[20,21]

* Corresponding author. Fax: + 81-75-383-2573. E-mail: kawasaki@moleng.kyoto-u.ac.jp.

10.1021/jp068390k CCC: $37.00
Published on Web 04/11/2007

2. Experimental Section

The CRDS apparatus used in the present study has been described elsewhere.[22] The system employed a photolysis laser (Spectra Physics, GCR-250 or Lambda Physik, OPTex PRO) and a probe laser (Spectra Physics, MOPO-SL, spectral resolution 0.2 cm^{-1}). After the photolysis laser pulse beam traversed a glass tube reactor, the probe laser pulse beam was injected nearly collinear to the axis of the photolysis laser through one of two high-reflectivity mirrors. The cavity ring-down mirrors (II−VI Co. or Research Electro-Optics, 7.8 mm diameter, and 1 m curvature) had a specified reflectivity of >0.999 and were mounted 1.04 m apart. Light leaking from the end mirror was detected by a photomultiplier tube (Hamamatsu Photonics, R212UH) through suitable colored glass filters (Edmund Optics). The length of the reaction region was 0.40 m. Temporal decay of the light intensity was recorded using a digital oscilloscope (Tektronix, TDL-714L, 8-bit resolution) and transferred to a personal computer. In the presence of an absorbing species, the light intensity within the cavity is given by expression 2:

$$I(t) = I_0 \exp(-t/\tau) = I_0 \exp(-t/\tau_0 - \sigma n c L_R t/L_C) \quad (2)$$

where I_0 and $I(t)$ are the light intensities at time 0 and t, τ is the cavity ring-down time with photolysis beam, τ_0 is the cavity ring-down time without photolysis laser light (typically 5 μs), L_R is the length of the reaction region (0.40 ± 0.02 m), L_C is the cavity length (1.04 m), c is the velocity of light, and n and σ are the concentration and the absorption cross section of absorbing species, respectively. A value of $\sigma_{BrO} = 1.21 \times 10^{-17}$ cm^2 $molecule^{-1}$ at 329.53 nm was used to calculate the absolute concentration of BrO at 298 K.[23] The temperature dependence of σ_{BrO} was considered when we performed the experiments at higher or lower temperatures. The reported temperature dependence of σ_{BrO} in the (7, 0) band head was applied to that of (9, 0) band head.[24] We calculated to be $\sigma_{BrO} = 1.6 \times 10^{-17}$ cm^2 $molecule^{-1}$ at 233 K, 1.5×10^{-17} cm^2 $molecule^{-1}$ at 253 K, 1.3×10^{-17} cm^2 $molecule^{-1}$ at 278 K, 1.1×10^{-17} cm^2 $molecule^{-1}$ at 313 K, and 1.0×10^{-17} cm^2 $molecule^{-1}$ at 333 K, respectively. The effect of the absorption of Br_2O, which was formed in the reaction of Br with BrO, was negligible. Using the IBM Chemical Kinetics Simulator it was estimated that the concentration of Br_2O was below 3×10^9 molecule cm^{-3} in the present experiments. The contribution of the formation of Br_2O_2 at lower temperature was also negligible because of the same reason. We assumed that the error in the estimation of the absolute concentration of BrO is within 23%, considering the uncertainties in reported absorption cross sections, pressure, mass flow rates, reaction path length and fluctuation of photolysis laser power. The vibrationally excited BrO, which was formed from the reaction of Br atom with O_3, was rapidly quenched by 100 or 200 Torr of N_2 or O_2 diluents, within 0.3−2.1 μs, based on the reported rate constants.[25]

Monitoring the CH_3O_2 time profiles with the use of the absorption at UV region was tested. However, non-negligible contributions of other absorptions were observed at the UV region, hence we did not adopt this system. Trying to monitor CH_3O_2 at near-IR region was also considered but failed, because of the small absorption cross section of CH_3O_2.

By varying the delay between the photolysis and probe laser pulses, the concentration of BrO was monitored as a function of delay time. Each ring-down trace was digitized with a time resolution of 20 ns. The digitized traces were transferred to a computer and averaged over 16 or 32 runs to calculate the ring-down rate, τ^{-1}.

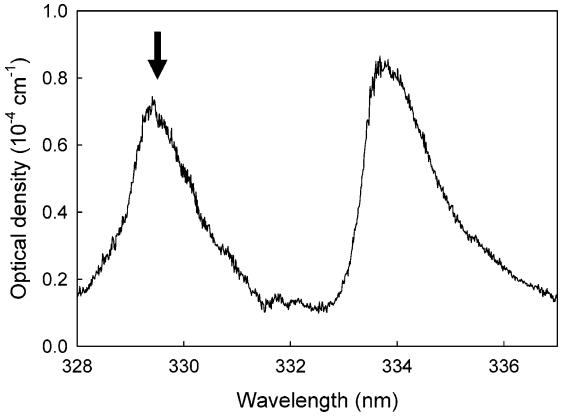

Figure 1. BrO spectrum measured from the photodissociation of the mixture of $O_3/O_2/Br_2$ at 266 nm. The arrow shows the peak of the (9, 0) band that is used for the present kinetic analysis.

Ozone concentrations were measured upstream of the reaction tube by monitoring the absorption at 253.7 nm ($\sigma = 1.15 \times 10^{-17}$ cm^2 $molecule^{-1}$)[23] using a separate low-pressure Hg lamp as a light source. Typical concentrations of O_3 and O_2 were $(1-10) \times 10^{15}$ and $(3-60) \times 10^{17}$ molecule cm^{-3}, respectively. The reaction of BrO with O_3[26] was not important in the present conditions, which is experimentally confirmed later. The self-reaction of BrO did not contribute to the decay of BrO significantly in the presence of excess ozone, because most of the products of the self-reaction are Br atoms, which rapidly regenerate BrO from the reaction of Br atoms with excess ozone.[27] The 213 nm output of the Nd^{3+}:YAG laser was used to dissociate CH_3Br to give CH_3 and Br. To generate the fifth harmonic laser light at 213 nm, a temperature controlled BBO crystal was used for mixing the fundamental and the fourth harmonic from the YAG laser. The typical laser intensity at 213 nm was 5 mJ $pulse^{-1}$. CH_3 reacted with O_2 to form CH_3O_2 within a few micro seconds as described later. Br reacted with O_3 to form BrO and O_2. Although O atoms were also formed from the photodissociation of O_3 at 213 nm, O atoms reacted with O_2 to form O_3. We confirmed the rapid regeneration of O_3, within 0.1 millisecond under typical conditions, using model calculations with the IBM Chemical Kinetics Simulator. Hence, no O atoms significantly affected the kinetic analysis under the present experimental conditions.

The 193 nm output of the ArF excimer laser was also used to dissociate both N_2O and CH_3COCH_3 to generate N_2 and $O(^1D)$, and $2CH_3$ and CO as an alternative method. Here the typical laser intensity was 7 mJ $pulse^{-1}$.

The reaction cell, consisting of a Pyrex glass tube (21 mm i.d.), was evacuated by the combination of an oil rotary pump, a mechanical booster pump and a liquid N_2 trap. The temperature of the gas flow region was controlled over the range 233−333 K by circulation of ethanol or water with a cooling circulator (Thomas, TRL 70 SLP and EYELA, NCB-2100). The difference between the temperature of the sample gas at the entrance and exit of the flow region was measured to be <1 K. The pressure in the cell was monitored by an absolute pressure gauge (Baratron, 622A or Copal, PA830). A slow flow of nitrogen gas was introduced at the ends of the ring-down cavity, close to the mirrors, in order to minimize deterioration caused by exposure to the reactants and the products in the cell. The total flow rate was adjusted (typically 2000 sccm) so that the gas in the cell was replaced completely within the 1 s time intervals between photolysis laser pulses.

Diluted sample gases for CH_3Br were prepared in glass gas bulbs with N_2 diluent. Then, the mixture gas was injected into

a glass reaction cell by the mass flow controllers (STEC, SEC-E40). Concentrations of these compounds in the reaction cell were calculated by the flow rates. All reagents were obtained from commercial sources. CH_3Br (>99%) was obtained from Tokyo Kasei Co. Br_2 (>99%) and CH_3COCH_3 (>99%) were obtained from Wako Pure Chemical. Br_2 and CH_3COCH_3 were subjected to freeze−pump−thaw cycling before use. CH_3Br, N_2O (high purity, Japan Air gases Co.), N_2 (>99.999%, Teisan Co.), and O_2 (>99.995%, Teisan Co.) were used without further purification.

3. Results

Self-Reaction of BrO. Radical concentrations of BrO were monitored at 329.53 nm, the band head of the $A^2\Pi_{3/2}\leftarrow X^2\Pi_{3/2}$ (9, 0) transition.[23,28] Figure 1 shows the cavity ring-down spectrum of BrO measured in the 266 nm photodissociation of a mixture of $Br_2/O_3/O_2$:

$$O_3 + h\nu\ (266\ \text{nm}) \rightarrow O(^1D) + O_2 \quad (3a)$$

$$\rightarrow O(^3P) + O_2 \quad (3b)$$

$$O(^1D) + O_2 \rightarrow O(^3P) + O_2 \quad (4a)$$

$$O(^3P) + Br_2 \rightarrow BrO + Br \quad (5)$$

At 100 Torr total pressure conditions of O_2 diluent, $O(^1D)$ was rapidly quenched by reaction 4a, hence no reactions concerning $O(^1D)$ were important. Using the system of $Br_2/O_3/O_2/h\nu$(266 nm) and a simple fitting equation for second order reactions, the rate constant of the self-reaction of BrO was determined to be $(2.6 \pm 0.6) \times 10^{-12}$ cm^3 molecule^{-1} s^{-1} at 298 K, in 100 Torr total pressure of O_2 diluent, which was the mean value of 5 independent experiments. Quoted uncertainty was 2σ. The concentrations of O_3 and Br_2 were $(0.8-1.6) \times 10^{13}$ and $(1.6 - 6.4) \times 10^{15}$ molecule cm^{-3}, respectively. The maximum concentrations of BrO were varied in the range of $(0.5-1.1) \times 10^{13}$ molecule cm^{-3}. The reaction of Br with O_3 was not important under the low O_3 concentration. The contribution of the regeneration of BrO was at most 14% compared with that of the total BrO formation based on kinetic simulations. The rate constant determined in the present study is in agreement with $(2.87 \pm 0.20) \times 10^{-12}$,[27] and the NASA recommended value, $(3.2 \pm 0.5) \times 10^{-12}$ cm^3 molecule^{-1} s^{-1} at 298 K.[23]

Reaction of BrO with CH_3O_2. CH_3O_2 radicals were generated by reactions 6 and 7 under an excess amount of O_2 (>10^{17} molecule cm^{-3}) within a few μs in our experimental conditions:

$$CH_3Br + h\nu(213\ \text{nm}) \rightarrow CH_3 + Br \quad (6)$$

$$CH_3 + O_2 + M \rightarrow CH_3O_2 + M \quad (7)$$

BrO was formed by the reaction of Br with O_3:

$$Br + O_3 \rightarrow BrO + O_2 \quad (8)$$

The BrO concentration profile was measured between 0.1−9.1 ms after the photolysis laser pulse. Figure 2 shows a typical rise and decay profile of the BrO concentration with CH_3Br of 5.5×10^{16} and O_3 of 5.5×10^{15} molecule cm^{-3} at 298 K in 200 Torr total pressure of O_2 diluent. Numerical models were compiled using the chemical equations listed in Table 1 in order to derive the rate constants of the reaction of BrO with CH_3O_2. The variable parameters were the initial concentrations of Br (=CH_3) and k_1 in the simulations so that the simulation results

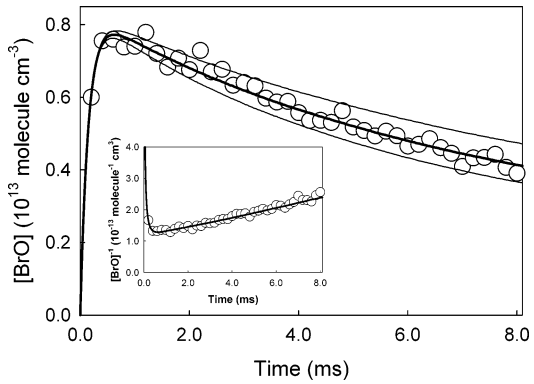

Figure 2. Typical rise and decay time profiles of BrO in the presence of CH_3O_2 at 298 K and 200 Torr total pressure of O_2 diluent. $[CH_3Br] = 5.5 \times 10^{16}$, $[O_3] = 5.5 \times 10^{15}$ and $[Br]_0 = [CH_3]_0 = 8.4 \times 10^{12}$ molecule cm^{-3}. The thick curve is the result of simulations. The thin curves show the uncertainty of 40%. The inset shows the temporal profiles of $[BrO]^{-1}$.

TABLE 1: Reactions Used in Kinetic Simulation for the Reaction of BrO with CH_3O_2 at 298 K and 200 Torr Total Pressure of O_2 Diluent in the Ozone System

reaction	rate constant (cm^6 molecule^{-2} s^{-1} or cm^3 molecule^{-1} s^{-1} or s^{-1})	ref
$Br + O_3 \rightarrow BrO + O_2$	1.2×10^{-12}	23
$BrO + CH_3O_2 \rightarrow$ products	best-fit parameter	this work
$2BrO \rightarrow 2Br + O_2$	2.6×10^{-12}	27
$\rightarrow Br_2 + O_2$	3.1×10^{-13}	27
$Br + BrO \rightarrow Br_2O$	2.5×10^{-13}	27[a]
$Br_2O + Br \rightarrow Br_2 + BrO$	4.0×10^{-11}	27
$BrO + O \rightarrow Br + O_2$	4.1×10^{-11}	49
$CH_3 + O_2 + M \rightarrow CH_3O_2 + M$	4.5×10^{-31}	23
$2CH_3O_2 \rightarrow 2CH_3O + O_2$	1.3×10^{-13}	49
$\rightarrow$ others	2.2×10^{-13}	49
$CH_3 + CH_3O_2 \rightarrow 2CH_3O$	2.0×10^{-11}	12
$CH_3O + O_2 \rightarrow HO_2 + HCHO$	1.9×10^{-15}	23
$CH_3O_2 + CH_3O \rightarrow$ products	1.0×10^{-12}	12
$CH_3O_2 + O \rightarrow CH_3O + O_2$	4.3×10^{-11}	50
$HO_2 + BrO \rightarrow HOBr + O_2$	2.4×10^{-11}	51
$HO_2 + Br \rightarrow HBr + O_2$	2.0×10^{-12}	23
$BrO + CH_3O \rightarrow$ products	5.5×10^{-11}	52
$Br + CH_3O \rightarrow$ products	5.3×10^{-11}	52
$Br + CH_3O_2 \rightarrow BrO + CH_3O$	4.4×10^{-13}	36
$Br + CH_3 \rightarrow CH_3Br$	1.5×10^{-11}	53[a]
$Br + Br + M \rightarrow Br_2 + M$	7.1×10^{-33}	54
$O + O_2 + M \rightarrow O_3 + M$	6.0×10^{-34}	23
$O + O_3 \rightarrow 2O_2$	8.0×10^{-15}	23
$O + Br_2 \rightarrow BrO + Br$	1.4×10^{-11}	27
diffusion rate	20 ± 10	this work

[a] Pressure corrections were performed assuming the reactions were in pure third order up to the pressure used.

reproduced the obtained decay time profiles of BrO. The diffusion loss rate from the detection region was determined to be (20 ± 10) s^{-1} from the best fits of simulation for several decays and was used for all other simulations. The diffusion loss rate determined in the present study was in agreement with that of our previous study on the reaction of BrO.[29]

The effects of the secondary reactions were carefully checked. Concentrations of CH_3O_2 and BrO were varied by using different concentrations of CH_3Br. The maximum concentration of BrO was varied in the range of $(3.2-8.0) \times 10^{12}$ molecule cm^{-3}. We found experimentally that the obtained k_1 had no dependence on the concentration of CH_3Br in the range of $(0.6-9.3) \times 10^{16}$ molecule cm^{-3}. These results indicate that k_1 is independent of the initial concentrations of CH_3 and Br. We also found experimentally that the value of k_1 had no dependence on the concentration of O_3 in the range of $(2.0 - 6.0) \times 10^{15}$

molecule cm^{-3}. No significant contribution to the first-order decay of BrO was observed as shown in the inset of Figure 2. These results indicate that the reactions of BrO with CH_3Br or O_3 did not occur in the present experimental conditions. The observed second-order decay is mostly attributable to the reaction of BrO with CH_3O_2 because both initial concentrations are almost the same and the self-reaction of BrO does not affect the decay of BrO as described previously.

With numerical simulation results and best-fit procedures, k_1 was observed to be $(6.2 \pm 2.5) \times 10^{-12}$ cm^3 molecule^{-1} s^{-1} at 200 Torr total pressure of O_2 diluent as shown in Figure 2, which was the mean value of 17 independent experiments. This rate constant is in good agreement with that of Aranda et al., $(5.7 \pm 0.6) \times 10^{-12}$ cm^3 molecule^{-1} s^{-1}.[14] The quoted uncertainty was derived by considering all uncertainties including the estimation of $[BrO]_0$, measurements in pressure, mass flow rates, reaction path length and simulation fittings. The each contribution to the BrO decay was 33−47% for reaction 1, 33−47% for the diffusion loss, 15−19% for the self-reaction of BrO, which were estimated by kinetic simulations. The contribution of secondary reactions, BrO + HO_2, BrO + CH_3O, BrO + O, and BrO + Br, to the decay of BrO were 1.4−1.5%, 0−1.2%, 0−2.6%, and 0−0.1%, respectively. The effect of possible reactive products from reaction 1 is considered below.

No significant pressure dependence of k_1 was observed within 40% of error bar range for the total pressure of 100, 107, 150, 188, and 200 Torr. A total of 16, 1, 1, 1, and 17 independent experiments were performed at each 100, 107 150, 188, and 200 Torr, respectively. The maximum concentration of BrO was varied in the range of $(3.2-8.0) \times 10^{12}$ molecule cm^{-3}. Hence, the present value of k_1 could be applicable to atmospheric modeling.

Because of the regeneration of BrO from the reaction of Br and O_3, the rate constant determined in the conditions described, the ''ozone system", might be a lower limiting value. Hence, an alternative method, photoirradiation of a mixture of N_2O/Br_2/CH_3COCH_3/O_2/N_2 at 193 nm, the ''N_2O system", was tested to obtain the rate constants of reaction 1 in the absence of O_3:

$$N_2O + h\nu\ (193\ nm) \rightarrow N_2 + O(^1D) \quad (9)$$

$$O(^1D) + N_2 \rightarrow O(^3P) + N_2 \quad (4b)$$

$$O(^3P) + Br_2 \rightarrow BrO + Br \quad (5)$$

$$CH_3COCH_3 + h\nu\ (193\ nm) \rightarrow 2CH_3 + CO \quad (10)$$

$$CH_3 + O_2 + M \rightarrow CH_3O_2 + M \quad (7)$$

Typical concentrations of CH_3COCH_3, N_2O, Br_2 and O_2 were $(0.3 - 1.8) \times 10^{16}$, $(1.6 - 3.4) \times 10^{17}$, $(1.3 - 2.2) \times 10^{15}$, and 6.4×10^{17} molecule cm^{-3}, respectively. A typical decay time profile of BrO in the presence of CH_3COCH_3 was shown in Figure 3. In the system, the reactions concerning N_2O, e.g., $O(^1D)$ + N_2O, were considered for simulation as shown in Table 2.

Initial concentration of CH_3 was estimated by the eq 11 and the initial concentration of $O(^1D)$, which was variable parameter in the fitting procedure

$$[CH_3]_0 = [O(^1D)]_0 \times \frac{2\sigma_{CH3COCH3}[CH_3COCH_3]_0}{\sigma_{N2O}[N_2O]_0} \quad (11)$$

$\sigma_{CH3COCH3}$, 2.88×10^{-18}, and σ_{N2O}, 8.95×10^{-20} cm^2 molecule^{-1} are quoted absorption cross sections at 193 nm at room temperature.[23,30] We could assume that reactions 9 and 10 occur in unity yield.[31,32]

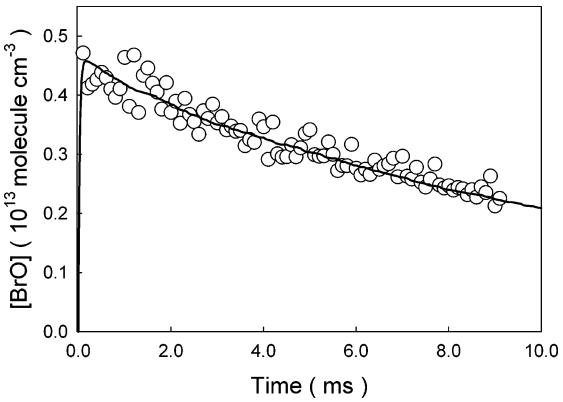

Figure 3. Typical rise and decay time profiles of BrO in the presence of CH_3O_2 at 298 K and 200 Torr total pressure of N_2 diluent. $[CH_3COCH_3] = 6.1 \times 10^{15}$, $[Br_2] = 2.2 \times 10^{15}$, and $[CH_3]_0 = 7.5 \times 10^{12}$ molecule cm^{-3}.

TABLE 2: Reactions Used in Kinetic Simulation for the Reaction of BrO with CH_3O_2 in the N_2O System[a]

reaction	rate constant (cm^6 molecule^{-2} s^{-1} or cm^3 molecule^{-1} s^{-1})	ref
BrO + CH_3O_2 → products	best-fit parameter	this work
Br_2 + O → BrO + Br	1.4×10^{-11}	27
$O(^1D) + N_2 \rightarrow O + N_2$	2.6×10^{-11}	23
$O(^1D) + O_2 \rightarrow O + O_2$	4.0×10^{-11}	23
$O(^1D) + O_2 \rightarrow O_3$	2.6×10^{-12}	55
$O(^1D) + N_2O \rightarrow 2NO$	6.7×10^{-11}	23
$O(^1D) + N_2O \rightarrow O + N_2O$	4.0×10^{-12}	49
$O(^1D) + N_2O \rightarrow N_2 + O_2$	4.9×10^{-11}	23
BrO + NO → Br + NO_2	2.1×10^{-11}	49
CH_3O_2 + NO → CH_3O + NO_2	7.7×10^{-12}	49
O + NO + M → NO_2 + M	1.0×10^{-31}	49
BrO + NO_2 + M → products + M	4.7×10^{-31}	49

[a] Reactions used in Table 1 were also included in the simulation.

With numerical simulation results and best-fit procedures in the N_2O system, k_1 was obtained to be $(5.6 \pm 2.2) \times 10^{-12}$ cm^3 molecule^{-1} s^{-1} at 298 K, 200 Torr total pressure of N_2 diluent, which was the mean value of 8 independent experiments. The maximum concentration of BrO was varied in the range of $(1.7 - 6.0) \times 10^{12}$ molecule cm^{-3}. The contributions to the BrO decay were 43−74% for reaction 1, 5.4−21% for the diffusion loss, 13−17% for the self-reaction of BrO, which were estimated by kinetic simulations. The contributions of secondary reactions, BrO + HO_2, BrO + CH_3O, BrO + NO_2, and BrO + Br were 4.3−7.2%, 1.1−3.2%, 0.7−3.5%, and 1.1−4.5%, respectively. The rate constant determined in this system is in excellent agreement with that of the "ozone system". Hence we can safely say that the BrO regeneration did not affect on the kinetic measurements in the ozone system.

We also conducted the experiments in the ozone system at 233−333 K. When analysis of the temperature dependence of k_1 was performed, all temperature-dependent reactions in Table 1 were taken into account. At 233 K, formation and decomposition of Br_2O_2, which was produced by the self-reaction of BrO,[27] were also included in the simulations, although the contributions to the kinetic analysis were negligible. Figure 4 shows the temporal profiles of $[BrO]^{-1}$ at 278, 298, and 333 K in 200 Torr total pressure of N_2 diluent. The rate constant, k_1, shows negative temperature dependence (see Table 3 and Figure 5). A total of 4, 4, 3, 17, 2, and 5 independent experiments were performed at each 233, 253, 278, 298, 313, and 333 K,

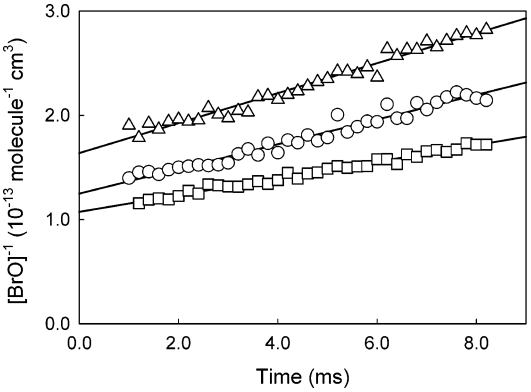

Figure 4. Temporal profiles of $[BrO]^{-1}$ at 278 K (triangle), 298 K (circle), and 333 K (square).

TABLE 3: Temperature Dependence of the Rate Constants for the Reaction of BrO with CH_3O_2 in 200 Torr Total Pressure of O_2 Diluent

temperature (K)	rate constant (10^{-12} cm^3 molecule^{-1} s^{-1})
233	15 ± 6
253	11 ± 4
278	8.8 ± 3.5
298	6.2 ± 2.5
313	6.8 ± 2.7
333	5.2 ± 2.1

respectively. The maximum concentration of BrO was varied in the range of $(0.3-1.1) \times 10^{13}$ molecule cm^{-3}. The Arrhenius analysis resulted in the activation energy of (-6.6 ± 0.6) kJ mol^{-1} and a pre-exponential factor of 4.6×10^{-13} cm^3 molecule^{-1} s^{-1}. The rate constant determined at 298 K is $(6.2 \pm 2.5) \times 10^{-12}$ cm^3 molecule^{-1} s^{-1}, which is in good agreement with the reported value, $(5.7 \pm 0.6) \times 10^{-12}$ cm^3 molecule^{-1} s^{-1} [14] as shown the triangle in Figure 5.

Products Branching Ratios. Considering that the results obtained from two independent systems, the O_3 system and the N_2O system, were essentially same, we concluded that the Br production path is not dominant in the reaction of BrO with CH_3O_2 at 298 K and 200 Torr of N_2 or O_2 diluent. Because if Br atoms were the dominant product, the decay of BrO should be slowed down in ozone system because of the regeneration of BrO by the rapid reaction of Br with O_3. The branching ratio for the Br formation was estimated to be below 0.4 considering all experimental uncertainties in the two systems.

We also tested the possible effect of reactive products, CH_3O and CH_2O_2, in the kinetics simulations. Even if the CH_3O forming branching ratio of reaction 1 is 0.4, only 0−4.5% decay change of BrO was observed. CH_2O_2 that would be formed from reaction 1c should not contribute to the kinetic analysis, because of the rapid decomposition to CO and H_2O with the rate constant of 60000 s^{-1}.[33] The reactions of CH_2O_2 with some species, e.g., Br atom, would not occur based on the simulations.

Formation of OBrO radicals from reaction 1b was investigated by trying to detect a CRDS signal of OBrO between 520 − 530 nm.[23] We conducted the detection of OBrO in the conditions of $[CH_3Br] = 4.1 \times 10^{16}$ and $[O_3] = 5.0 \times 10^{15}$ molecule cm^{-3} at 298 K and 200 Torr total pressure of O_2 diluent. However, we could not find any evidence of OBrO. Based on our detection limit, which was derived using the reported absorption cross section of OBrO at 521.6 nm,[34] and from simulated time profiles of OBrO, the upper limit of the branching ratio of reaction 1b was estimated to be <0.1.

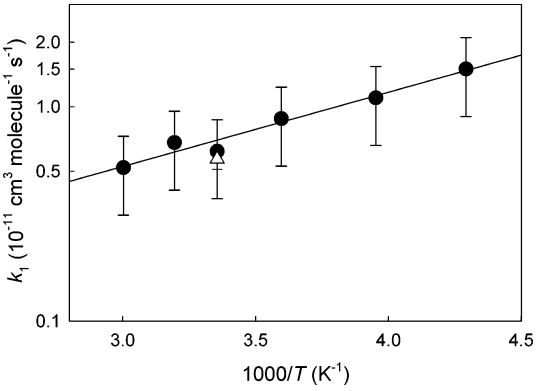

Figure 5. Temperature dependence of the rate constant of the reaction of BrO with CH_3O_2 at 233−333 K. The triangle from Aranda et al. (ref 14).

HOBr and CH_3OBr could not be detected because the absorption cross-sections of these products in the UV region are too small to observe.[35]

Reaction of Br atom with CH_3O_2. We performed a kinetic study of the BrO formation from the reaction of Br with CH_3O_2 in the absence of O_3 at 298 K, 100 Torr of N_2 or O_2 diluent conditions:

$$CH_3O_2 + Br \rightarrow CH_3O + BrO \qquad (12a)$$

A BrO signal was not observed in the 213 nm photodissociation of the mixture of $[CH_3Br] = (3.5 - 5.2) \times 10^{16}$ and $[O_2] = (0.6 - 3.2) \times 10^{18}$ molecule cm^{-3} in the absence of O_3. The present experimental results were simulated using the IBM Chemical Kinetics Simulator. The upper limit of the rate constant for the BrO formation path from the reaction of CH_3O_2 with Br was estimated to be $<5 \times 10^{-13}$ cm^3 molecule^{-1} s^{-1} at 298 K, 100 Torr of N_2 or O_2 diluent conditions. Hence, the reaction of Br with CH_3O_2 did not affect the kinetic analysis of the reaction, BrO and CH_3O_2. The present rate constant of the BrO formation path from the reaction of CH_3O_2 and Br is in fair agreement with that of Aranda et al., 4.4×10^{-13} cm^3 molecule^{-1} s^{-1}.[36] A recent theoretical study by Francisco and Crowley suggests that the CH_3O_2 and Br reaction is dominated by the formation of the CH_3OOBr intermediate that can be stabilized by collisions to be the final product or decomposes to CH_2OO and HBr, CH_3O and BrO, and CH_2O and HOBr.[37]

4. Discussion

Our present results show that the Br formation path (1a) and OBrO formation path (1b) are not dominant. These results are in good agreement with those reported by Aranda et al.[14] The present results may be understood if the stability of the intermediates of reaction 1 is $CH_3OOOBr > CH_3OOBrO$ as reported by Guha and Francisco,[15] because OBrO could be formed only from the CH_3OOBrO intermediate:

$$CH_3O_2 + BrO \rightarrow CH_3OOOBr^* \rightarrow \text{products} \qquad (1)$$

$$CH_3OOBrO^* \rightarrow \text{products}$$

No OBrO formation is consistent with the results of other reactions $XO + CH_3O_2$.[13,16]

The negative temperature dependence of k_1 is consistent with that for BrO with HO_2[23] and with the intermediate formation mechanism in reaction 1 as proposed by Guha and Francisco.[15] Since no pressure dependence was observed between 100 and 200 Torr total pressure, the hot CH_3OOOBr^* complex is not

stabilized under our present pressure conditions (100−200 Torr) to decompose into products, e.g., $CH_2O + HOOBr$. Considering the previously reported results, that is, the rate constant determined at 1 Torr total pressure of He diluent is essentially the same as the present results at 100−200 Torr total pressure of N_2 or O_2 diluent and also the theoretical result that the CH_3OOOBr would decompose to other products, we believe that the CH_3OOOBr complex is not the final product under present experimental conditions.

A comparison of the rate constants for the reactions of XO (X═I, Br and Cl) with CH_3O_2 shows a trend of increasing reactivity in the order, $k(IO) \gg k(BrO) > k(ClO)$, 7.0×10^{-11} for IO,[13] 0.6×10^{-11} for BrO, and 0.2×10^{-11} cm^3 molecule^{-1} s^{-1} for ClO[23]. The same trend was recognized for the self-reactions of XO.[23] These observations could be explained by the ionization potential (I_p) for XO, 9.7 eV for IO,[38] 10.5 eV for BrO[39] and 10.9 eV for ClO.[40] These reactions may occur via the attack to the O atom in CH_3O_2 by XO. The order, $k(BrO) > k(ClO)$, for the rate constants of XO with CH_3O_2 could also be explained by the stability of the intermediate, CH_3OOOX. The ΔH of these complexes were calculated to be −93.7 kJ mol^{-1} for CH_3OOOBr[15] and −86.6 kJ mol^{-1} for CH_3OOOCl.[41] The experimentally determined activation energies of the reactions of XO with CH_3O_2, which should be the sum of all reaction paths, are −6.6 kJ mol^{-1} for BrO and 0.9 kJ mol^{-1} for ClO,[16] which may indicate that the CH_3OOOBr is more stabilized than CH_3OOOCl, and hence, the reaction of BrO with CH_3O_2 favorably proceeds this intermediate mechanism.

5. Atmospheric Implications

Bromine-Catalyzed Ozone Loss Processes. In an extensive global model study by Pyle and co-workers,[42] the importance of bromine catalyzed ozone loss in the troposphere was emphasized, causing reductions of 4−6% in the northern hemisphere and up to 30% at high latitudes in the southern hemisphere. Using the rate coefficient from Aranda et al.,[14] reaction 1 was included in their model, and deemed to be unimportant compared with the cycle:

$$Br + O_3 \rightarrow BrO + O_2 \quad (8)$$

$$BrO + HO_2 \rightarrow HOBr + O_2 \quad (13)$$

$$HOBr + h\nu \rightarrow OH + Br \quad (14)$$

$$\text{net } O_3 + HO_2 \rightarrow OH + 2O_2$$

However, the model chemistry used in their model study contains relatively few non-methane hydrocarbons and is likely to underestimate the concentration of CH_3O_2 (and RO_2) as well as underestimating the rate coefficient of reaction 1, particularly in the upper troposphere and lower stratosphere. Pyle's work identifies two major sources of Br_x, volatilization of sea-salt and photooxidation of bromocarbons. Sea-salt gives rise to high Br_x at mid and high latitudes at the surface and in the mid troposphere at high latitudes, whereas photooxidation of bromocarbons is the dominant source in the upper troposphere and also the lower stratosphere. Measurements of CH_3O_2 radicals in isolation are rare, and most measurement techniques yield a sum of peroxy radicals (RO_2). Inspections of RO_2/HO_2 ratios in the regions where Br_x levels are likely to be elevated are few, Creasey et al.[43] reported ratios of around 3/1 at Mace Head (51°N) and Salisbury et al.[44] report ratios of around 5/2 at Cape Grim (40 °S). In order to assess the potential importance of reaction 1, a comparison of the two rate coefficients k_1 and k_{13} from 300 to 225 K is instructive and is summarized in Table 4,

TABLE 4: Comparison of the Ratios for k_{13}/k_1 from 233 to 298 K[a]

	k_{13}/k_1 this work			k_{13}/k_1
temperature (K)	averaged	upper limit	lower limit	ref 14
298	3.7	8.7	1.9	4.0
278	3.0	7.1	1.5	4.6
253	2.9	6.8	1.4	5.6
233	2.6	6.5	1.2	6.7

[a] The temperature dependent k_{13} are taken from ref 42. k_1 from ref 14 is fixed to the value determined at 298 K.

using a value[42] for $k_{13} = 3.7 \times 10^{-12} \exp[(544.9 \pm 99.8)/T]$. First, the data in Table 4 show that by using the present temperature-dependent values and the temperature-independent value of Aranda et al.[14] the potential importance of reaction 1 and the general reaction between BrO and RO_2 could be underestimated considerably at subambient temperatures. Second, the ratio of k_{13}/k_1 lies between 4 and 2.5 (although there are wide error limits), and hence the ratio of RO_2:HO_2 required for the two reactions with BrO to be equal will also lie between 4 and 2.5. Given the atmospheric field measurements available, this suggests that the reaction of BrO with RO_2 (if k_1 is representative) will compete with the reaction between BrO and HO_2 throughout the marine boundary layer. With reference to the work of Pyle,[42] it would seem that reaction 1 may therefore play a non negligible role in ozone destruction throughout the troposphere at high latitudes and at the surface and upper troposphere at mid-latitudes. Assuming that CH_3O_2 is representative of RO_2 and it would seem so based on analogous studies of the reaction of RO_2 and IO radicals,[13] this class of reaction will be important.

In the upper troposphere and lower stratosphere, the concentration of peroxy radicals is enhanced by Cl initiated oxidation of hydrocarbons,[45−47] and many global models do not include either this additional oxidation route or a complete representation of VOC. Inspection of model fields[47] incorporating these new kinetic data into a column model suggest that 20−30% of CH_3O_2 conversion to CH_3O will be via reaction 1 in the troposphere and 10% in the stratosphere.

CH_3Br Formation Process. Wingenter et al.[48] have reported unexplained enhancements of CH_3Br during Arctic Boundary Layer ozone depletion episodes and speculated where this source may be from. They have ruled out marine and urban sources and production in snow. Intriguingly they suggested that reaction 1 or 12 could be the missing source:

$$CH_3O_2 + BrO \rightarrow CH_3Br + O_3 \quad (1f)$$

$$CH_3O_2 + Br \rightarrow CH_3Br + O_2 \quad (12b)$$

Moreover, they assert that a branching ratio for reaction 1f of just 0.001 using the rate constant of Aranda (determined at 298 K) would lead to a production of CH_3Br of 40 kt a year, making it a significant source. This work has shown that the rate coefficient for reaction 1f at 253 K (more typical of the Arctic and indeed the upper free troposphere) could be twice as large as that at room temperature and therefore the value used by Wingenter et al.[48] Clearly a small branching ratio of 0.001 for reaction 1f cannot be ruled out by these studies, hence the reaction remains a potential source of CH_3Br.

6. Conclusions

The rate constant of the reaction of BrO with CH_3O_2 was determined to be $(6.2 \pm 2.5) \times 10^{-12}$ cm^3 molecule^{-1} s^{-1} at

298 K and 100−200 Torr of N_2 or O_2 diluent. Temperature dependence of the rate constant was investigated at 233−333 K. The present work improves our understanding of the kinetics of BrO with CH_3O_2 in two respects. First, we reported the first measurements of the temperature dependence of the rate constant at 233−333 K. We also revealed that no pressure dependence of the rate constant of reaction 1 was observed at 100−200 Torr of N_2 and O_2 diluent. Second, we concluded that Br and OBrO formation paths from reaction 1 are not dominant. The CH_3OOOBr formation mechanism is more likely in the atmospheric conditions to produce other products. The present results reveal that the reaction of BrO with CH_3O_2 will affect the halogen chemistry in the troposphere, contributing to ozone destruction cycles. If the reaction is representative of the interaction of BrO with RO_2, then this class of reaction will compete with the reaction of BrO with HO_2 in ozone destruction cycles.

Acknowledgment. S.E. is grateful to the JSPS Research Fellowship for Young Scientists. M.K. and D.E.S. thank the Daiwa Adrian Foundation for funding. The Biogeochemistry Research Centre is a joint venture between the School of Chemistry and the Departments of Earth Science and Geography.

References and Notes

(1) Saiz-Lopez, A.; Shillito, J. A.; Coe, H.; Plane, J. M. C. *Atoms. Chem. Phys.* **2006**, *11*, 1513.
(2) Calvert, J. G.; Lindberg, S. E. *Atoms. Environ.* **2004**, *38*, 5087.
(3) Kanaya, Y.; Akimoto, H. *Chem. Rec.* **2002**, *2*, 199.
(4) Salawitch, R. J. *Nature* **2006**, *439*, 275.
(5) Carpenter, L. J. *Chem. Rev.* **2003**, *103*, 4953.
(6) Saiz-Lopez, A.; Plane, J. M. C.; Shillito, J. A. *Geophys. Res. Lett.* **2004**, *31*, L03111,doi:10.1029/2003GL018956.
(7) Hausmann, M.; Platt, U. *J. Geophys. Res.* **1994**, *99*, 25399.
(8) Kreher, K.; Johnston, P. V.; Wood, S. W.; Platt, U. *Geophys. Res. Lett.* **1997**, *24*, 3021.
(9) Tas, E.; Peleg, M.; Matveev, V.; Zingler, J.; Luria, M. *J. Geophys. Res.* **2005**, *110*, D11304. [Online early access]. DOI: 10.1029/2004JD005665.
(10) Fleming, Z. L.; Monks, P. S.; Rickard, A. R.; Heard, D. E.; Bloss, W. J.; Seakins, P. W.; Still, T. J.; Sommariva, R.; Pilling, M. J.; Morgan, R.; Green, T. J.; Brough, N.; Mills, G. P.; Penkett, S. A.; Lewis, A. C.; Lee, J. D.; Saiz-Lopez, A.; Plane, J. M. C. *Atoms. Chem. Phys.* **2006**, *20*, 2193.
(11) Burkert, J.; Andres-Hernandez, M. D.; Stobener, D.; Burrows, J. P.; Wessenmayer, M.; Kraus, A. *J. Geophys. Res.* **2001**, *106*, 5457.
(12) Bale, C. S. E.; Canosa-Mas, C. E.; Shallcross, D. E.; Wayne, R. P. *Phys. Chem. Chem. Phys.* **2005**, *7*, 2164.
(13) Enami, S.; Yamanaka, T.; Hashimoto, S.; Kawasaki, M.; Nakano, Y.; Ishiwata, T. *J. Phys. Chem. A* **2006**, *110*, 9861.
(14) Aranda, A.; LeBras, G.; LaVerdet, G. L.; Poulet, G. *Geophys. Res. Lett.* **1997**, *24*, 2745.
(15) Guha, S.; Francisco, J. S. *J. Chem. Phys.* **2003**, *118*, 1779.
(16) Helleis, F.; Crowley, J. N.; Moortgat, G. K. *J. Phys. Chem.* **1993**, *97*, 11464.
(17) O'Keefe, A.; Deacon, D. A. G. *Rev. Sci. Instrum.* **1988**, *59*, 2544.
(18) Wheeler, M. D.; Newman, S. M.; Orr-Ewing, A. J.; Ashfold, M. N. R. *J. Chem. Soc., Faraday Trans.* **1998**, *94*, 337.
(19) Yu, T.; Lin, M. C. *J. Am. Chem. Soc.* **1993**, *115*, 4371.
(20) Enami, S.; Nakano, Y.; Hashimoto, S.; Kawasaki, M.; Aloisio, S.; Francisco, J. S. *J. Phys. Chem. A* **2004**, *108*, 7785.
(21) Enami. S.; Ueda, J.; Nakano, Y.; Hashimoto, S.; Kawasaki, M. *J. Geophys. Res.* **2004**, *109*, D05309.
(22) Enami, S.; Hoshino, Y.; Ito, Y.; Hashimoto, S.; Kawasaki, M.; Wallington, T. J. *J. Phys. Chem. A* **2006**, *110*, 3546.
(23) Sander, S. P.; Friedl, R. R.; Ravishankara, A. R.; Golden, D. M.; Kolb, C. E.; Kurylo, M. J.; Huie, R. E.; Orkin, V. L.; Molina, M. J.; Moortgat G. K.; Finlayson-Pitts, B. J. *Chemical Kinetics and Photochemical Data for Use in Stratospheric Modeling*; Evaluation 14; Jet Propulsion Laboratory: Pasadena, CA, 2003.
(24) Gilles, M. K.; Turnipseed, A. A.; Burkholder, J. B.; Ravishankara, A. R.; Solomon, S. *J. Phys. Chem. A* **1997**, *101*, 5526.
(25) Ninomiya, Y.; Hashimoto, S.; Kawasaki, M.; Wallington, T. J. *Int. J. Chem. Kinet.* **2000**, *32*, 125.
(26) Rattigan, O. V.; Cox, R. A.; Jones, R. L. *J. Chem. Soc., Faraday Trans.* **1995**, *91*, 4189.
(27) Harwood, M. H.; Rowley, D. M.; Cox, R. A.; Jones, R. L. *J. Phys. Chem. A* **1998**, *102*, 1790.
(28) Fleischmann, O. C.; Hartmann, M.; Burrows, J. P.; Orphal, J. *J. Photochem. Photobiol., A* **2004**, *168*, 117.
(29) Nakano, Y.; Goto, M.; Hashimoto, S.; Kawasaki, M.; Wallington, T. J. *J. Phys. Chem. A* **2001**, *105*, 11045.
(30) Seki, K.; Okabe, H. *J. Phys. Chem.* **1992**, *96*, 3345.
(31) Nishida, S.; Takahashi, K.; Matsumi, Y.; Taniguchi, N.; Hayashida, S. *J. Phys. Chem. A* **2004**, *108*, 2451.
(32) Takahashi, K.; Nakayama, T.; Matsumi, Y.; Osamura, Y. *J. Phys. Chem. A* **2004**, *108*, 8002.
(33) Mariq, M. M.; Szente, J. J.; Kaiser, E. W.; Shi. J. *J. Phys. Chem.* **1994**, *98*, 2089.
(34) Knight, G.; Ravishankara, A. R.; Burkholder, J. B. *J. Phys. Chem. A* **2000**, *104*, 11121.
(35) Keller-Rudek, H.; Moortgat, G. K. *MPI-Mainz-UV-VIS Spectral Atlas of Gaseous Molecules*. www.atmosphere.mpg.de/spectral-atlas-mainz (accessed Nov 2006).
(36) Aranda, A.; Laverdet, G.; Le Bras, G.; Poulet, G. *J. Chim. Phys.* **1998**, *95*, 963.
(37) Francisco, J. S.; Crowley, J. N. *J. Phys. Chem. A* **2006**, *110*, 3778.
(38) Monks, P. S.; Stief, L. J.; Tardy, D. C.; Liebman, J. F.; Zhang, Z.; Kuo, S.-C.; Klemm, R. B. *J. Phys. Chem.* **1995**, *99*, 16566.
(39) Monks, P. S.; Stief, L. J.; Krauss, M.; Kuo, S. C.; Klemm, R. B. *Chem. Phys. Lett.* **1993**, *211*, 416.
(40) Thorn, R. P., Jr.; Stief, L. J.; Kuo, S.-C.; Klemm, R. B. *J. Phys. Chem.* **1996**, *100*, 14178.
(41) Drougas, E.; Jalbout, A. F.; Kosmas, A. M. *J. Phys. Chem. A* **2003**, *107*, 11386.
(42) Yang, X.; Cox, R. A.; Warwick, N. J.; Pyle, J. A.; Carver, G. D.; O'Connor, F. M.; Savage, N. H. *J. Geophys. Res.* **2005**, *110*, D23311, doi: 10.1029/2005JD006244.
(43) Creasey, D. J.; HalfordMaw, P. A.; Heard, D. E.; Pilling, M. J.; Whitaker, B. J. *J. Chem. Soc., Faraday Trans.* **1997**, *93*, 2907.
(44) Salisbury, G.; Monks, P. S.; Bauguitte, S.; Bandy, B. J.; Penkett, S. A. *J. Atmos. Chem.* **2002**, *41*, 163.
(45) Lary, D. J. *Atoms. Chem. Phys.* **2005**, *5*, 227.
(46) Lary, D. J.; Toumi, R. *J. Geophys. Res. Atoms.* **1997**, *102*, 23421.
(47) Lary, D. J.; Shallcross, D. E. *J. Geophys. Res. Atmos.* **2000**, *105*, 19771.
(48) Wingenter, O. W.; Sive, B. C.; Blake, D. R.; Rowland, F. S.; Ridley, B. A. *Geophys. Res. Lett.* **2003**, *30*, 22 and 160. [Online early access]. DOI: 10.1029/2003GL018159.
(49) Atkinson, R.; Baulch, D. L.; Cox, R. A.; Crowley, J. N.; Hampson, R. F., Jr.; Kerr, J. A.; Rossi, M. J.; Troe, J. *IUPAC Subcommittee on Gas Kinetic Data Evaluation for Atmospheric Chemistry*; IUPAC: 2004.
(50) Zellner, R.; Hartmann, D.; Karthauser, J.; Rhasa, D.; Weibring, G. *J. Chem. Soc., Faraday Trans. 2* **1988**, *84*, 549.
(51) Bloss, W. J.; Rowley, D. M.; Cox, R. A.; Jones, R. L. *Phys. Chem. Chem. Phys.* **2002**, *4*, 3639.
(52) Shah, D.; Canosa-Mas, C. E.; Hendy, N. J.; Scott, M. J.; Vipond, A, Wayne, R. P. *Phys. Chem. Chem. Phys.* **2001**, *3*, 4932.
(53) Krasnoperov, L. N.; Mehta, K. *J. Phys. Chem. A* **1999**, *103*, 8008.
(54) Jenkin, M. E.; Cox, R. A.; Mellouki, A.; Le Bras, G.; Poulet, G. *J. Phys. Chem.* **1990**, *94*, 2927.
(55) Castellano, E.; Schumacher, H. J. *Z. Phys. Chem.* **1969**, *65*, 62.